Journal of
Synchrotron
Radiation

ISSN 0909-0495

Received 12 September 2009
Accepted 7 February 2010

In situ observation of Ni–Mo–S phase formed on $NiMo/Al_2O_3$ catalyst sulfided at high pressure by means of Ni and Mo *K*-edge EXAFS spectroscopy

Naoto Koizumi,[a]* Yusuke Hamabe,[a] Sungbong Jung,[a] Yasuhiro Suzuki,[a] Shohei Yoshida[a] and Muneyoshi Yamada[b]

[a]Department of Applied Chemistry, Graduate School of Engineering, Tohoku University, Aoba 6-6-07, Aramaki, Aoba-ku, Sendai 980-8579, Japan, and [b]Akita National College of Technology, 1-1 Iijima-Bunkyo-cho, Akita 011-8511, Japan. E-mail: koizumi@erec.che.tohoku.ac.jp

To obtain direct evidence of the formation of the Ni–Mo–S phase on $NiMo/Al_2O_3$ catalysts under high-pressure hydrodesulfurization conditions, a high-pressure EXAFS chamber has been constructed and used to investigate the coordination structure of Ni and Mo species on the catalysts sulfided at high pressure. The high-pressure chamber was designed to have a low dead volume and was equipped with polybenzimidazole X-ray windows. Ni *K*-edge $k^3\chi(k)$ spectra with high signal-to-noise ratio were obtained using this high-pressure chamber for the $NiMo/Al_2O_3$ catalyst sulfided at 613 K and 1.1 MPa over a wide k range (39.5–146 nm^{-1}). The formation of Ni–Mo and Mo–Ni coordination shells was successfully proved by Ni and Mo *K*-edge EXAFS measurement using this chamber. Interatomic distances of these coordination shells were almost identical to those calculated from Ni *K*-edge EXAFS of NiMo/C catalysts sulfided at atmospheric pressure. These results support the hypothesis that the Ni–Mo–S phase is formed on the Al_2O_3-supported NiMo catalyst sulfided under high-pressure hydrodesulfurization conditions.

Keywords: EXAFS spectroscopy; high-pressure chamber; Ni–Mo–S phase; hydrodesulfurization; $NiMo/Al_2O_3$ catalysts.

1. Introduction

Topsøe *et al.* (Topsøe & Clausen, 1984; Topsøe *et al.*, 1986; Clausen *et al.*, 1996) proposed that the Co–Mo–S phase was formed on $CoMo/Al_2O_3$ catalysts by sulfiding at atmospheric pressure as a hydrodesulfurization (HDS) active phase and, since that time, many studies have shown detailed investigations of the formation of binary sulfide clusters by means of Mössbauer emission spectroscopy, EXAFS and FT-IR spectroscopy coupled with NO adsorption (Topsøe *et al.*, 1981; Wivel *et al.*, 1981; Clausen *et al.*, 1981; Koizumi *et al.*, 1996; Koizumi, Yamazaki, Hatanaka & Yamada, 1997; Yamada *et al.*, 1999; Cattaneo *et al.*, 2001; Okamoto *et al.*, 2003; Dugulan *et al.*, 2004, 2008). One of the most important pieces of experimental evidence for the formation of the Co–Mo–S and Ni–Mo–S phases is the observation of Co–Mo and Ni–Mo coordination shells by *in situ* Co and Ni *K*-edge EXAFS measurement at liquid-N_2 temperature of the catalysts sulfided at atmospheric pressure (Bouwens *et al.*, 1990, 1991; Louwers & Prins, 1992). However, the catalyst is exposed to a high-pressure sulfiding atmosphere under industrial HDS conditions. The coordination structure of the promoter atoms under these industrial HDS conditions has never been investigated. It is also noted here that these EXAFS spectra were mainly obtained using carbon-supported catalysts rather than Al_2O_3-supported catalysts. Carbon support improves the signal-to-noise ratio of Co and Ni *K*-edge EXAFS spectra because carbon is more transparent to X-rays compared with Al_2O_3. Furthermore, the k range applied to Fourier transforms (FTs) of EXAFS spectra was limited to a maximum of around 110 nm^{-1} (Bouwens *et al.*, 1991; Louwers & Prins, 1992), which could weaken contributions from Co–Co (Ni–Ni) and/or Co–Mo (Ni–Mo) scattering pairs in their EXAFS spectra because the scattering of electrons by these atoms mainly contributes in these k ranges. A limited k range also means that the number of independent parameters for curve-fitting analysis is reduced.

In our research it was previously shown that, by means of *in situ* diffuse reflectance FT-IR spectroscopy (DRIFTS) coupled with NO adsorption, Mo surface sites disappeared by the addition of small amounts of Co and/or Ni when the $CoMo/Al_2O_3$ and $NiMo/Al_2O_3$ catalysts were sulfided at pressures higher than 1.1 MPa (Koizumi *et al.*, 1996; Koizumi, Yamazaki, Hatanaka & Yamada, 1997; Yamada *et al.*, 1999; Koizumi, Yamazaki, Iijima & Yamada, 1997). Mo *K*-edge EXAFS measurement using a high-pressure chamber revealed that the

Mo sulfide species was hardly sintered by high-pressure sulfiding pretreatment (Koizumi, Yamazaki, Hatanaka & Yamada, 1997; Yamada *et al.*, 1999). The results suggested that the Co–Mo–S and Ni–Mo–S phases were more effectively formed by high-pressure sulfiding pretreatment (*i.e.* under industrially relevant HDS conditions) rather than by atmospheric pressure sulfiding pretreatment. However, further experimental evidence is necessary to confirm this point because that work used DRIFTS coupled with NO adsorption, and Mo *K*-edge EXAFS does not provide direct information about the coordination structure of the Co and Ni promoters.

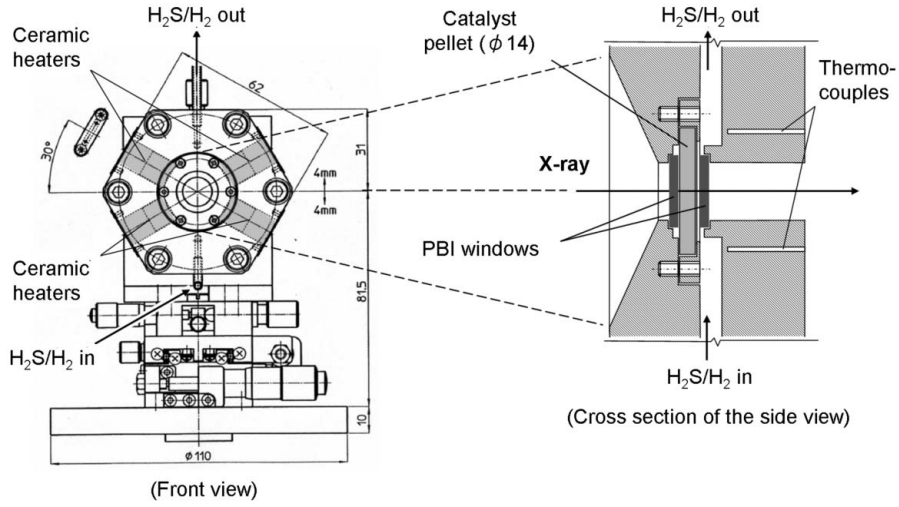

Figure 1
High-pressure chamber used for EXAFS measurement. Units of dimensions: mm.

To obtain direct evidence for the formation of the Co–Mo–S and Ni–Mo–S phases on the Al_2O_3-supported catalysts under industrial HDS conditions, *in situ* Co and Ni *K*-edge EXAFS measurement on the catalysts sulfided at high-pressures are necessary. In this work a high-pressure EXAFS chamber has been constructed that provides EXAFS spectra with a high signal-to-noise ratio even in the *k* range above 110 nm^{-1}. The effect of the Ni:Mo molar ratio on the Ni *K*-edge EXAFS of the $NiMo/Al_2O_3$ catalyst sulfided at 613 K and 1.1 MPa was systematically investigated using this newly constructed chamber. Mo *K*-edge EXAFS of the catalyst was also investigated in the present study.

2. Experimental

2.1. High-pressure EXAFS chamber

The EXAFS chamber constructed in the present study was made of SUS 316 stainless steel, and designed for transmission measurement. This high-pressure chamber was designed to have a low dead volume (~6 mm) between X-ray windows as shown in Fig. 1. The chamber design minimizes X-ray absorption by high-pressure H_2S/H_2 because of this low dead volume. During sulfiding pretreatment using a 5% H_2S/H_2 stream at 1.1 MPa, for instance, X-ray absorption by 5% H_2S/H_2 between X-ray windows was no more than 3.4% at 8.33 keV for this chamber, whereas it accounted for around 64% in the chamber used in our previous Mo *K*-edge EXAFS studies (Koizumi, Yamazaki, Hatanaka & Yamada, 1997; Yamada *et al.*, 1999).

A beryllium disc is a conventional X-ray window of choice (Dalla Betta *et al.*, 1984; Kampers *et al.*, 1989; Shirai *et al.*, 1995; Jentoft *et al.*, 1996; Grunwaldt *et al.*, 2005). However, commercial beryllium discs usually contain small amounts of Cu impurity that would seriously contaminate the Ni *K*-edge EXAFS spectra at higher *k* ranges. This contamination could be the main reason for the limited *k* range applied to FTs of Ni *K*-edge EXAFS spectra of the NiMo/C catalysts reported previously (Louwers & Prins, 1992). To extend the available *k* range for FT, a Cu-free polybenzimidazole (PBI; AZ Electronic MaterialsLtd, diameter 14.5 mm) disc was used as the X-ray window for Ni *K*-edge EXAFS measurement. For Mo *K*-edge EXAFS measurement, a high-purity beryllium disc (NGK, Cu impurity level < 0.015%, diameter 15 mm) was used as the X-ray window because of the absence of such contamination of the spectra. A catalyst pellet (diameter 14 mm, $\Delta\mu t = \sim 0.7$) was placed between the X-ray windows. Micro ceramic heaters (Sakaguchi EH Voc) were located inside the chamber. The temperature around the catalyst pellet was monitored by four thermocouples inserted into the chamber.

2.2. Signal-to-noise ratio of Ni *K*-edge EXAFS measured using the high-pressure chamber

To check the performance of the newly constructed high-pressure chamber, polycrystalline NiO was subjected to Ni *K*-edge EXAFS measurement using the chamber.

Fig. 2(*A*) compares Ni *K*-edge $k^3\chi(k)$ spectra of polycrystalline NiO (Wako Pure Chemicals, purity >99%) measured with and without using the high-pressure chamber at the synchrotron radiation facility SPring-8 (see §2.3) under ambient conditions. The chamber was equipped with PBI windows. The crystallinity of the sample was checked and confirmed by powder X-ray diffraction analysis. These two Ni *K*-edge $k^3\chi(k)$ spectra were identical over the whole *k* range (10–200 nm^{-1}). Use of the high-pressure chamber provided the Ni *K*-edge $k^3\chi(k)$ spectrum with a signal-to-noise ratio comparable with the spectrum measured without the chamber. In other words, use of the high-pressure chamber hardly deteriorated the signal-to-noise ratio of the Ni *K*-edge EXAFS spectra.

To show the advantage of using PBI X-ray windows, the polycrystalline NiO was then subjected to Ni *K*-edge EXAFS measurement using the chamber equipped with beryllium windows. The obtained spectrum was compared with that measured when the chamber was equipped with PBI windows

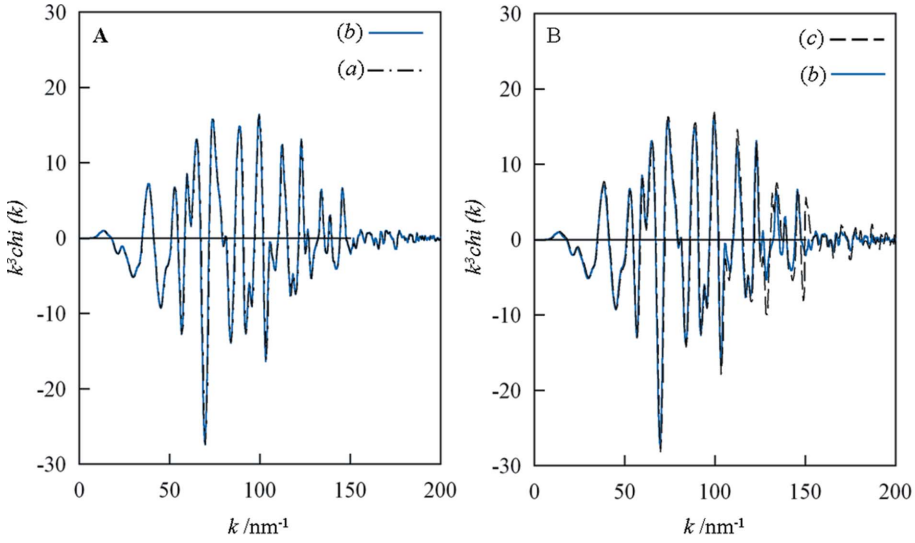

Figure 2
Ni *K*-edge $k^3\chi(k)$ spectra of the polycrystalline NiO. X-ray absorption spectra were measured with (*b* and *c*) and without (*a*) using the high-pressure chamber at ambient temperature. The chamber used was equipped with PBI (*b*) and beryllium (*c*) windows.

(Fig. 2*B*). These two Ni *K*-edge $k^3\chi(k)$ spectra were almost identical in the k range below 100 nm^{-1}. However, the EXAFS oscillation became stronger in the higher k range when the beryllium windows were used. A different type of oscillation was also observed in this range. The difference between these two spectra occurred because of the superimposition of the Cu *K*-edge X-ray absorption spectrum of small amounts of Cu impurity (<0.015%) in the beryllium windows. For such contamination of the spectrum, the FT range should be limited to a maximum of around 100 nm^{-1}. This contamination will be more serious in the Ni *K*-edge EXAFS spectra of catalysts because the EXAFS oscillation is usually much weaker in the higher k range compared with the polycrystalline NiO (see §3.1). Use of the PBI windows effectively extends the FT range of the Ni *K*-edge EXAFS towards a higher k range.

2.3. *In situ* Ni and Mo *K*-edge EXAFS measurement

EXAFS measurements were conducted at synchrotron radiation facilities in Japan [Photon Factory (PF) and SPring-8]. Ni *K*-edge EXAFS spectra were measured at beamlines BL9C (PF) and BL14B2 (SPring-8) with ring energies of 2.5 and 8 GeV, respectively. The X-rays passed through a Si(111) double-crystal monochromator and focused onto the sample. The EXAFS data were collected in transmission mode using I_0 and I ionization chambers filled with 100% N_2 and 15% Ar/N_2, respectively. Mo *K*-edge EXAFS spectra were measured at beamline NW10A (PF-AR) with a ring energy of 6.5 GeV. The X-rays were monochromated with a Si(311) monochromator and detected by two ionization chambers filled with 50% Ar/N_2 for I_0 and 100% Ar for I.

The high-pressure chamber was connected to a flow apparatus equipped with mass flow controllers (Brooks Instruments, 5850E) and back-pressure regulators (TESCOM). Before EXAFS measurement, a 5% H_2S/H_2 (>99.99999%) stream was introduced into the chamber at ambient temperature (1.1 MPa, 60 ml min^{-1}). The chamber was then heated to 613 K (Ni *K*-edge EXAFS) or 673 K (Mo *K*-edge EXAFS) at a rate of 10 K min^{-1}. During sulfiding pretreatment, EXAFS measurements were carried out at 298 K, 373 K, 473 K, 573 K, 613 K and 673 K. The temperature was kept constant during measurements that required ~20–30 min to acquire the spectrum. After reaching 613 K (or 673 K), this temperature was kept constant until no further spectral change was observed (90–170 min depending on the sample). Finally, the chamber was cooled down to room temperature under a flowing H_2S/H_2 stream followed by EXAFS measurement at ambient temperature. In this paper, only the spectra measured at ambient temperature after sulfiding pretreatment are presented because of the relatively lower signal-to-noise ratio of the spectra measured during sulfiding pretreatment.

2.4. EXAFS analysis

Observed X-ray absorption spectra were analyzed in a conventional manner including background subtraction and normalization followed by Fourier filtering using Rigaku XAFS data analysis software (*REX2000*). Contributions from coordination shells in the Fourier-transformed Ni and Mo *K*-edge $k^3\chi(k)$ spectra were then inverse Fourier transformed with a Hanning-type window function into k space. The structural parameters of each coordination shell were determined by a non-linear least-square fitting in k space. Backscattering amplitudes and phase shifts of the Ni–O, Ni–S, Ni–Ni, Ni–Mo, Mo–S, Mo–Mo and Mo–Ni coordination shells were calculated using the *FEFF8.4* code (Ankudinov *et al.*, 1998) using NiO (Ni–O) (Rooksby, 1948), NiS_2 (Ni–S) (Nowack *et al.*, 1991), Ni (Ni–Ni) (Swanson & Tatge, 1953), $Ni_{2.5}Mo_6S_8$ (Ni–Mo and Mo–Ni) (Chang *et al.*, 1987) and MoS_2 (Mo–S and Mo–Mo) (Dickinson & Pauling, 1923) structures. In the non-linear least-square fitting of Ni *K*-edge EXAFS spectra, the inner potential (E_0) and the Debye–Waller factor (σ^2) of each coordination shell were fixed at the values obtained from polycrystalline NiO, Ni_3S_2 (Aldrich, purity >99.7%) and Ni foil. This was necessary to make the number of parameters comparable with the number of independent parameters (N_{idp}) (Stern, 1993) defined by the k and R ranges as follows,

$$N_{idp} = (2\Delta k \Delta R/\pi) + 2. \quad (1)$$

Curve-fitting analysis was then conducted, where the reducing factors (S_0^2) (Roy & Gurman, 1999) for the Ni–O, Ni–S and Ni–Ni coordination shells were fixed at 0.47, 0.73 and 0.85, respectively. These values were obtained by fitting the Ni–O,

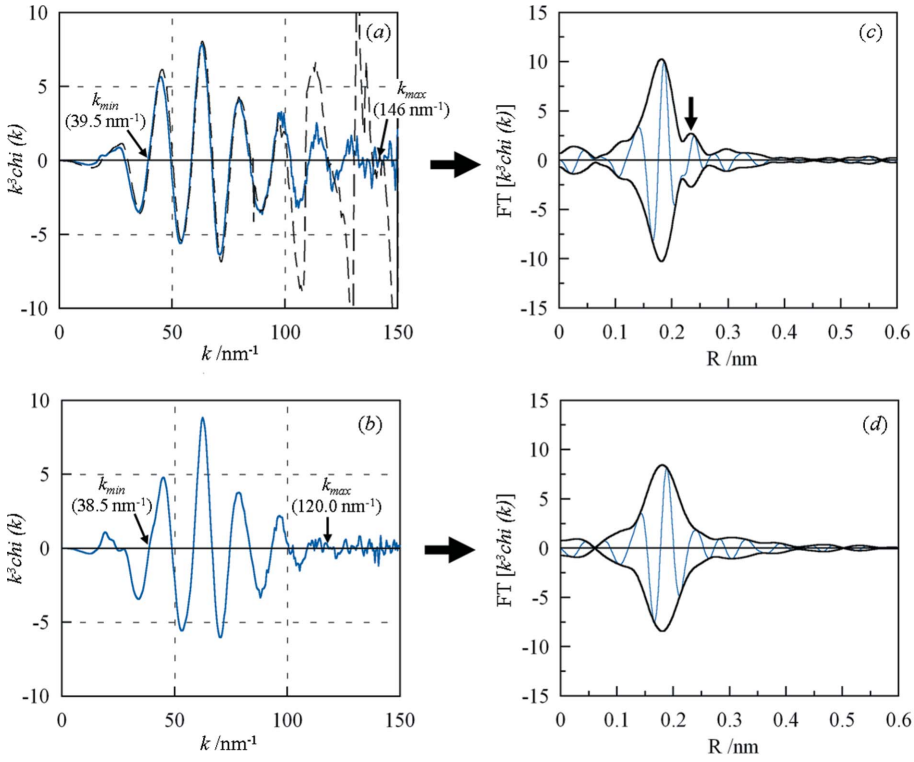

Figure 3
Ni *K*-edge $k^3\chi(k)$ and their FT-EXAFS spectra of the NiMo(0.4) (*a*, *c*) and Ni(3) (*b*, *d*) catalysts. X-ray absorption spectra were measured at ambient temperature after sulfiding pretreatment at 613 K and 1.1 MPa using the high-pressure chamber equipped with PBI windows, whereas the broken line in (*a*) represents the Ni *K*-edge $k^3\chi(k)$ spectrum of the NiMo(0.4) catalyst measured using the chamber equipped with beryllium windows. The FT range is indicated by k_{min} and k_{max} in the Ni *K*-edge $k^3\chi(k)$ spectra.

Ni–S and Ni–Ni contributions in the Ni *K*-edge EXAFS of polycrystalline NiO, Ni_3S_2 and Ni foil. Similarly, the reducing factors were determined for Mo–S (0.91) and Mo–Mo (0.97) using polycrystalline MoS_2 (Wako Pure Chemicals, purity >99.5%). The quality of the fitting was calculated using the *R*-factor (R_f) defined by the following equation,

$$R_f\,(\%) = \left\{ \sum_i \left[k^3\chi_i^{obs}(k) - k^3\chi_i^{cal}(k)\right]^2 / \sum_i \left[k^3\chi_i^{obs}(k)\right]^2 \right\} \times 100. \quad (2)$$

2.5. Catalyst preparation

The catalysts used were homemade $NiMo/Al_2O_3$ catalysts that had various Ni:Mo molar ratios. These catalysts were prepared by a successive incipient wetness impregnation method from $Ni(NO_3)_2{\cdot}6H_2O$ (Wako Pure Chemicals, purity >99.9%) and $(NH_4)_6Mo_7O_{24}{\cdot}4H_2O$ (Wako Pure Chemicals, purity >99%) as Ni and Mo sources, respectively. First, γ-Al_2O_3 powder (Nippon Ketjen, 314 m^2 g^{-1}, 0.78 ml g^{-1}) was impregnated with an aqueous $(NH_4)_6Mo_7O_{24}{\cdot}4H_2O$ solution, followed by drying and calcination. The thus obtained Mo/Al_2O_3 catalyst was then impregnated with an aqueous $Ni(NO_3)_2{\cdot}6H_2O$ solution followed by drying and calcination to obtain the $NiMo/Al_2O_3$ catalyst. Detailed preparation procedures have been reported elsewhere (Koizumi, Yamazaki, Iijima & Yamada, 1997; Kasahara *et al.*, 1994). The Ni:Mo molar ratio was varied from 0.2 to 1.5, whereas the Mo content was kept constant (15 mass% MoO_3). The Ni/Al_2O_3 catalyst was prepared in a similar manner using the aqueous $Ni(NO_3)_2{\cdot}6H_2O$ solution. In this paper, the $NiMo/Al_2O_3$ and Ni/Al_2O_3 catalysts are denoted as NiMo(*X*) and Ni(*Y*) catalysts, where *X* and *Y* stand for the Ni:Mo molar ratio and NiO content in mass%, respectively. For the sake of comparison, the carbon-supported NiMo catalyst was also prepared using nitrilotriacetic acid (Dojindo Molecular Technologies) according to the procedure described in a previous study (Louwers & Prins, 1992). HSAG-3000 high-surface-area graphite (Lonza, 300 m^2 g^{-1}, 0.25 cm^3 g^{-1}) was used as support. The Ni:Mo molar ratio of this catalyst was 0.48.

3. Results and discussion

3.1. Ni *K*-edge EXAFS of the NiMo catalyst measured with the high-pressure chamber

To demonstrate the advantage of using PBI windows in Ni *K*-edge EXAFS measurements on $NiMo/Al_2O_3$ catalysts, the spectra measured using the chamber equipped with the PBI or beryllium windows were firstly compared. Fig. 3(*a*) displays Ni *K*-edge $k^3\chi(k)$ spectra of the NiMo(0.4) catalyst measured at ambient temperature after sulfiding pretreatment at 613 K and 1.1 MPa. The chamber used in this measurement was equipped with PBI windows. EXAFS oscillations were clearly visible even in the higher k range in this spectrum. The maximum k value for FT reached 146 nm^{-1} (indicated by k_{max} in the figure). The Ni *K*-edge $k^3\chi(k)$ spectrum of NiMo(0.4) catalyst measured with the same high-pressure chamber, but equipped with the beryllium windows instead of PBI windows, is shown in the same figure (Fig. 3*a*, broken line). Compared with the spectra shown in Fig. 2(*B*), the Ni *K*-edge $k^3\chi(k)$ spectrum was more seriously contaminated with Cu *K*-edge X-ray absorption above 100 nm^{-1}. Use of the PBI X-ray windows was indispensable for obtaining the Ni *K*-edge $k^3\chi(k)$ spectrum of the NiMo catalysts in the k range higher than 100 nm^{-1}.

The Ni *K*-edge $k^3\chi(k)$ spectrum of the NiMo(0.4) catalyst measured using the chamber equipped with the PBI windows was then Fourier transformed in the range indicated by k_{min} and k_{max} in the figure. The Fourier-transformed Ni *K*-edge $k^3\chi(k)$ (FT-EXAFS) spectrum is shown in Fig. 3(*c*). In this spectrum a main peak was observed at around 0.18 nm (not

Table 1
Fitting results for the Ni *K*-edge $k^3\chi(k)$ spectra of the Ni catalyst as a function of NiO content (*Y*).

CN: coordination number. *R*: distance. E_0: inner potential. σ^2: Debye–Waller factor. N_{idp}: number of independent parameters defined by equation (1). EXAFS measurements were conducted at ambient temperature after high-pressure sulfiding pretreatment.

Y	Scattering pair	CN	*R* (nm)	E_0 (eV)†	σ^2 (10^{-5} nm^2)†	Δk (nm^{-1})	N_{idp}	R_f (%)
3.0 mass%	Ni–O	0.9	0.203	−8.728	1.44	38.5–120	8	0.08
	Ni–S	4.5	0.222	−4.213	7.40			
	Ni–Ni	0.7	0.253	−2.669	2.81			
4.7 mass%	Ni–O	0.4	0.209	−8.728	1.44	39.0–137	9	0.18
	Ni–S	4.9	0.222	−4.213	7.40			
	Ni–Ni	0.6	0.253	−2.669	2.81			
10 mass%	Ni–O	0.9	0.207	−8.728	1.44	39.5–132	9	0.25
	Ni–S	4.6	0.221	−4.213	7.40			
	Ni–Ni	0.8	0.252	−2.669	2.81			

† E_0 and σ^2 were not fitted.

phase-shift corrected). A weak shoulder peak was also observed at around 0.24 nm (not phase-shift corrected) as indicated by the arrow. The Ni(3) catalyst was also subjected to Ni *K*-edge EXAFS measurement with the chamber equipped with the PBI windows as a reference. The Ni *K*-edge $k^3\chi(k)$ spectrum of this catalyst is shown in Fig. 3(*b*). The EXAFS oscillation of this spectrum was more rapidly attenuated compared with the Ni *K*-edge $k^3\chi(k)$ spectrum of the NiMo(0.4) catalyst, resulting in a lower k_{max} for this spectrum. The FT-EXAFS spectrum of the Ni(3) catalyst showed a broader peak at around 0.18 nm (not phase-shift corrected). Furthermore, the shoulder peak was not observed in the FT-EXAFS spectrum of the Ni(3) catalyst. This suggests that some kind of specific coordination shell is formed on the NiMo/Al_2O_3 catalyst. To clarify the origin of this shoulder peak in relation to the formation of the Ni–Mo–S phase, the effect of the Ni:Mo molar ratio on the Ni *K*-edge EXAFS of the NiMo/Al_2O_3 catalyst was then investigated because this ratio is thought to be a crucial parameter for the formation of the Ni–Mo–S phase.

3.2. Effect of the Ni:Mo molar ratio on the Ni *K*-edge EXAFS

Fig. 4 shows FT-EXAFS spectra of NiMo/Al_2O_3 catalysts with different Ni:Mo molar ratios [NiMo(*X*) catalysts] in comparison with spectra of Ni/Al_2O_3 catalysts with different NiO content [Ni(*Y*) catalysts]. These spectra were measured at ambient temperature after sulfiding at 613 K and 1.1 MPa.

3.2.1. Ni(*Y*) catalysts. In the FT-EXAFS spectra of the Ni(*Y*) catalysts, broad peaks centered at around 0.18 nm (not phase-shift corrected) appeared irrespective of Ni content. Curve-fitting analysis showed that these spectra were well fitted with Ni–O, Ni–S and Ni–Ni coordination shells (not shown here). Table 1 summarizes optimized structural parameters of these coordination shells. Interatomic distances of the Ni–S and Ni–Ni coordination shells of the Ni(3) catalyst were 0.222 and 0.253 nm, respectively. These distances were almost identical to those of the coordination shells of polycrystalline Ni_3S_2. However, the coordination number of the Ni–Ni shell (∼1) was smaller than that of the shell of the polycrystalline Ni_3S_2 (4) (Parise, 1980), suggesting the formation of small Ni_3S_2 species. The formation of small Ni_3S_2 species was consistent with previous results on Ni/C catalysts sulfided at atmospheric pressure (Louwers & Prins, 1992). The coordination number and interatomic distance of these shells were identical among the Ni(*Y*) catalysts, showing that the formation of the Ni_3S_2 species was hardly affected by the Ni content.

On the other hand, the Ni—O distances (0.203–0.209 nm) were in between those of $NiAl_2O_4$ (0.181 nm; Areán & Viñuela, 1985) and NiO (0.210 nm; Rooksby, 1948), suggesting that two types of Ni oxide species were formed on this catalyst. Relatively longer Ni—O distances of the Ni(4.7) and Ni(10) catalysts further suggested that NiO species was preferentially formed on the catalysts with higher Ni content.

3.2.2. NiMo(*X*) catalysts. In contrast to the spectra of the Ni/Al_2O_3 catalysts, FT-EXAFS spectra of the NiMo/Al_2O_3 catalysts changed depending on the Ni:Mo molar ratio. The main peak became broader with increasing Ni:Mo molar ratio. Furthermore, the shoulder peak was no longer clearly visible in the spectrum of the catalyst with high Ni:Mo molar ratio.

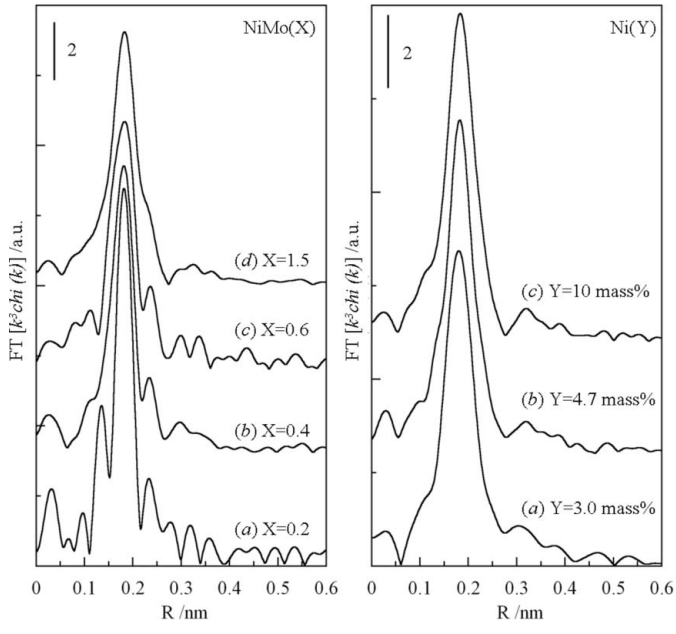

Figure 4
Effect of the Ni:Mo molar ratio on Ni *K*-edge FT-EXAFS spectra of the NiMo(*X*) catalysts. Ni *K*-edge FT-EXAFS spectra of the Ni(*Y*) catalysts are shown in the right-hand side figure as a reference. X-ray absorption spectra were measured at ambient temperature after sulfiding pretreatment at 613 K and 1.1 MPa using the chamber equipped with the PBI windows.

To investigate the effect of the Ni:Mo molar ratio, curve-fitting analysis was conducted with and without using the Ni–Mo coordination shell. The spectrum of the NiMo(0.4) catalyst was fitted first with the Ni–O, Ni–S and Ni–Ni coordination shells as in the case of the Ni(3) catalyst, *i.e.* without using the Ni–Mo coordination shell. Best-fitting results are shown in Figs. 5(*a*) and 5(*c*). The Ni *K*-edge $k^3\chi(k)$ spectrum was not well fitted with these coordination shells (Fig. 5*a*). The R_f value was 28 times higher than that for the Ni(3) catalyst (2.8% *versus* 0.1%). Furthermore, the shoulder peak at around 0.24 nm (phase shift not corrected) in the FT-EXAFS spectrum was underestimated when fitted without using the Ni–Mo coordination shell (Fig. 5*c*). Then the spectrum was fitted using the Ni–O, Ni–S, Ni–Ni and Ni–Mo coordination shells. The R_f value was significantly reduced by the addition of the Ni–Mo coordination shell in the fitting analysis (Fig. 5*b*). The shoulder peak in the FT-EXAFS spectrum was also fitted well in this case (Fig. 5*d*). Similarly, the Ni–Mo coordination shell was necessary to obtain good fitting results for other NiMo catalysts. The structural parameters of each coordination shell are summarized in Table 2. The interatomic distance of the Ni–Mo coordination shell was in the 0.273–0.276 nm range. This distance was comparable with those reported for the Ni–Mo coordination shell of the Ni–Mo–S phase formed on the NiMo/C catalyst sulfided at atmospheric pressure (Louwers & Prins, 1992). This suggests that the Ni–Mo–S phase is formed on the NiMo/Al_2O_3 catalyst sulfided at high pressure. It is also noted that the spectrum of the NiMo(0.2) catalyst was well fitted with only the Ni–S and Ni–Mo coordination shells, suggesting that the Ni–Mo–S phase is selectively formed at low Ni:Mo molar ratios.

Table 2
Fitting results for Ni *K*-edge $k^3\chi(k)$ spectra of the NiMo(*X*) catalyst as a function of the Ni:Mo molar ratio (*X*).

See Table 1 for explanation of symbols.

X	Scattering pair	CN	*R* (nm)	E_0 (eV)†	σ^2 (10^{-5} nm^2)†	Δk (nm^{-1})	N_{idp}	R_f (%)
0.2 mol mol^{-1}	Ni–S	7.1	0.220	−4.213	7.40	39.0–142	8	3.85
	Ni–Mo	0.5	0.273	0	3.60			
0.4 mol mol^{-1}	Ni–O	1.5	0.203	−8.728	1.44	39.5–146	9	0.25
	Ni–S	4.8	0.220	−4.213	7.40			
	Ni–Ni	0.4	0.245	−2.669	2.81			
	Ni–Mo	0.7	0.273	0	3.60			
0.6 mol mol^{-1}	Ni–O	2.1	0.203	−8.728	1.44	40.0–131	9	0.05
	Ni–S	3.9	0.219	−4.213	7.40			
	Ni–Ni	0.9	0.249	−2.669	2.81			
	Ni–Mo	1.0	0.276	0	3.60			
1.5 mol mol^{-1}	Ni–O	1.0	0.206	−8.728	1.44	40.0–148	11	0.25
	Ni–S	4.5	0.221	−4.213	7.40			
	Ni–Ni	0.7	0.249	−2.669	2.81			
	Ni–Mo	0.7	0.274	0	3.60			

† E_0 and σ^2 were not fitted.

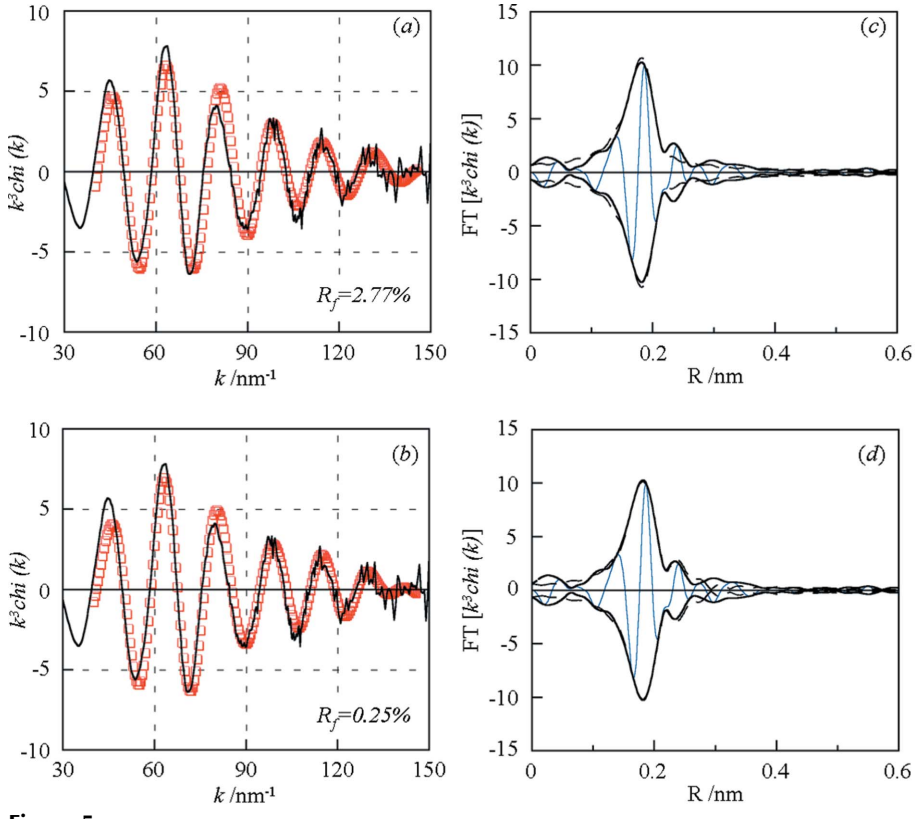

Figure 5
Best-fitting results for the NiMo(0.4) catalyst (fitted data are represented by squares). The R_f value defined by equation (2) is also included in the figures. (*a*), (*c*) Fitting was conducted using the Ni–O, Ni–S and Ni–Ni coordination shells. (*b*), (*d*) Fitting was conducted using the Ni–Mo coordination shell in addition to the Ni–O, Ni–S and Ni–Ni coordination shells.

For the catalyst with Ni:Mo molar ratio higher than 0.4, the Ni–O and Ni–Ni coordination shells were also necessary for obtaining good fitting results. The Ni–O and Ni–Ni distances of the NiMo(0.6) and NiMo(1.5) catalysts were almost identical to those of the Ni(*Y*) catalysts. Thus, Ni oxide and Ni_3S_2 species were concomitantly formed on these catalysts above this ratio. On the other hand, the Ni—Ni distance of the NiMo(0.4) catalyst (0.245 nm) was 0.008 nm shorter than that of the Ni(3) catalyst. This difference was beyond the error of the curve-fitting analysis (±0.004 nm). This suggests that the nature of Ni_3S_2-like species on the NiMo(0.4) catalyst is slightly different from

Table 3
Fitting results for Mo-edge $k^3\chi(k)$ spectra of the NiMo(X) catalyst as a function of the Ni:Mo molar ratio (X).

CN: coordination number. R: distance. E_0: inner potential. σ^2: Debye–Waller factor. R_f: R-factor EXAFS measurements were conducted at ambient temperature after high-pressure sulfiding pretreatment. N_{idp}: number of independent parameters defined by equation (1).

X	Scattering pair	CN	R (nm)	E_0 (eV)	σ^2 (10^{-5} nm^2)	Δk (nm^{-1})	N_{idp}	R_f (%)
0 mol mol^{-1}	Mo–S	5.0	0.241	0.056	3.14	30.0–151	13	0.46
	Mo–Mo	3.5	0.316	−1.633	3.84			
0.2 mol mol^{-1}	Mo–S	5.6	0.241	−0.606	3.36	30.0–150	14	0.36
	Mo–Mo	3.6	0.316	0.197	3.84			
0.6 mol mol^{-1}	Mo–S	5.7	0.241	−0.501	3.14	30.0–150	14	0.40
	Mo–Mo	3.8	0.316	0.486	3.60			
1.5 mol mol^{-1}	Mo–S	5.8	0.241	0.279	2.92	30.5–148	13	0.33
	Mo–Mo	3.8	0.317	−0.312	3.25			

those on the Ni(Y) catalysts. Because the Ni–Mo–S phase was suggested to be selectively formed at a low Ni:Mo molar ratio (0.2), it is likely that only a small amount of Ni is involved in the formation of the Ni_3S_2-like species on the NiMo(0.4) catalyst. This may lead to the formation of quite small Ni_3S_2 clusters, which perturbs their Ni—Ni distance.

Louwers & Prins (1992) investigated the Ni K-edge EXAFS spectra of the NiMo/C catalysts sulfided at atmospheric pressure. Based on curve-fitting analysis, they suggested that the Ni–Mo–S phase was selectively formed at Ni:Mo molar ratios up to 0.48. This is apparently different from our Ni K-edge EXAFS results, where Ni oxide and Ni_3S_2 species were concomitantly formed on the NiMo(0.4) catalyst. Different speciation of Ni may be related to different types of support used in this work. On the other hand, based on *in situ* Mössbauer measurements, Wivel *et al.* (1981) suggested that Co oxide species as well as the Co–Mo–S phase was formed at low Co:Mo molar ratios ($\leq$0.27) on the $CoMo/Al_2O_3$ catalyst sulfided at atmospheric pressure. Taking their results into consideration, our Ni K-edge EXAFS results imply that high-pressure sulfiding pretreatment effectively converts Ni oxide species into the Ni–Mo–S phase, although further investigations are necessary to clarify the effect of high-pressure sulfiding.

3.2.3. Effect of the Ni:Mo molar ratio on Mo *K*-edge EXAFS. To investigate the formation of the Ni–Mo–S phase from a different point of view, the effect of the Ni:Mo molar ratio on Mo K-edge EXAFS of the $NiMo/Al_2O_3$ catalyst was further investigated in this work.

Fig. 6 shows Fourier-transformed Mo K-edge $k^3\chi(k)$ (Mo K-edge FT-EXAFS) spectra of the NiMo(X) catalysts. These spectra were measured at ambient temperature after sulfiding pretreatment at 673 K and 1.1 MPa. Two distinct peaks were clearly observed in these spectra at around 0.2 and 0.3 nm (not phase-shift corrected). These peaks are well known as the Mo–S and Mo–Mo coordination shells of MoS_2 species (Koizumi, Yamazaki, Hatanaka & Yamada, 1997; Yamada *et al.*, 1999; Bouwens *et al.*, 1990; Fujikawa *et al.*, 2006; Nicosia & Prins, 2005). Optimized structural parameters of these coordination shells obtained from curve-fitting analysis are summarized in Table 3. The interatomic distances of these coordination shells were identical to those of the shells of polycrystalline MoS_2, whereas the coordination number of the Mo–Mo shell ($\sim$4) was smaller than that of the shell of the polycrystalline MoS_2 (6) (Dickinson & Pauling, 1923). Therefore, MoS_2 species forming on these catalysts had a smaller basal plane size as suggested in previous studies (Koizumi, Yamazaki, Hatanaka & Yamada, 1997; Yamada *et al.*, 1999; Bouwens *et al.*, 1990; Fujikawa *et al.*, 2006; Nicosia & Prins, 2005). The coordination number of the Mo–S and Mo–Mo shells increased slightly with the Ni:Mo ratio, suggesting that the crystallinity of the MoS_2 species improved by the addition of the Ni (Co) promoter (Kasahara *et al.*, 1994; Boudart *et al.*, 1983). It is also noted that the quality of fitting hardly improved by the addition of the Mo–Ni coordination shell in the fitting analysis. This is reasonable in view of the structure of the Ni–Mo–S phase, in which Ni atoms are located only at the edge sites of MoS_2 species. Most of the Mo atoms will be coordinated to S and Mo atoms, not Ni atoms in the Ni–Mo–S phase.

An attempt was then made to extract the Mo–Ni coordination shell by subtracting the Mo K-edge $k^3\chi(k)$ of the Mo/Al_2O_3 catalyst from those of the $NiMo/Al_2O_3$ catalysts. Fig. 7 shows the thus obtained Fourier-transformed $\Delta k^3\chi(k)$

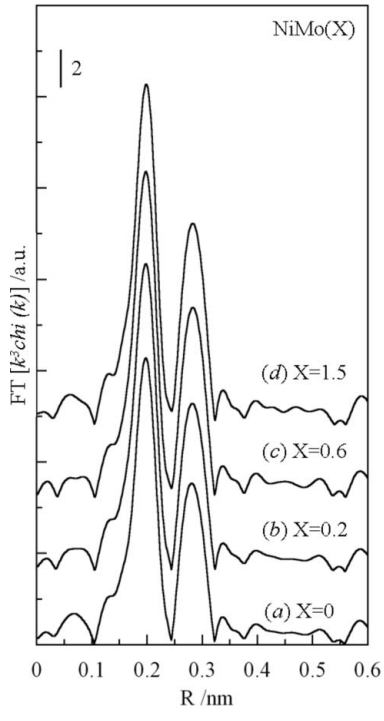

Figure 6
Effect of the Ni:Mo molar ratio on the Mo K-edge FT-EXAFS spectra of the NiMo(X) catalysts. X-ray absorption spectra were measured at ambient temperature after sulfiding pretreatment at 673 K and 1.1 MPa using the chamber equipped with PBI windows.

spectra. Two peaks were still observed at around 0.2 and 0.3 nm in these spectra. These peaks grew with the Ni:Mo molar ratio, probably due to the improvement of the crystallinity of the MoS_2 species by the addition of the Ni promoter. Furthermore, a shoulder peak became clearly detectable at around 0.25 nm (not phase-shift corrected) in all these spectra, suggesting the formation of the Mo–Ni coordination shell. Curve-fitting analysis was conducted on $\Delta k^3\chi(k)$ spectra using the Mo–S, Mo–Ni and Mo–Mo coordination shells. Fitting results for the NiMo(0.6) catalyst are shown in Fig. 8 as an example. Good fitting was obtained in both k and R space using these coordination shells. Optimized structural parameters of the Mo–Ni coordination shell are summarized in Table 4. The interatomic distances of this coordination shell were almost identical to those of the Ni–Mo coordination shell. In other words, Mo K-edge EXAFS measurement also supported the hypothesis that the Ni–Mo–S phase is formed on the Al_2O_3 supported NiMo catalyst sulfided under high-pressure conditions. It is also stressed here that the formation of the Mo–Ni coordination shell has never been reported even for the NiMo/C catalyst sulfided at atmospheric pressure.

Table 4
Fitting results for Mo K-edge $\Delta k^3\chi(k)$ spectra of NiMo(X) catalysts.

See Table 3 for explanation of symbols.

X	Scattering pair	CN	R (nm)	E_0 (eV)	σ^2 (10^{-5} nm^2)	Δk (nm^{-1})	N_{idp}	R_f (%)
0.2 mol mol^{-1}	Mo–S	0.4	0.244	3.770	3.25	27.0–144	12	1.37
	Mo–Ni	0.2	0.272	0.962	7.74			
	Mo–Mo	0.2	0.324	6.824	2.92			
0.6 mol mol^{-1}	Mo–S	0.7	0.243	0.001	2.21	24.0–145	14	1.14
	Mo–Ni	0.2	0.275	5.437	2.92			
	Mo–Mo	0.7	0.321	1.422	3.36			
1.5 mol mol^{-1}	Mo–S	0.9	0.242	0.607	2.21	32.5–150	15	1.71
	Mo–Ni	0.2	0.277	8.168	2.70			
	Mo–Mo	0.6	0.319	1.150	1.94			

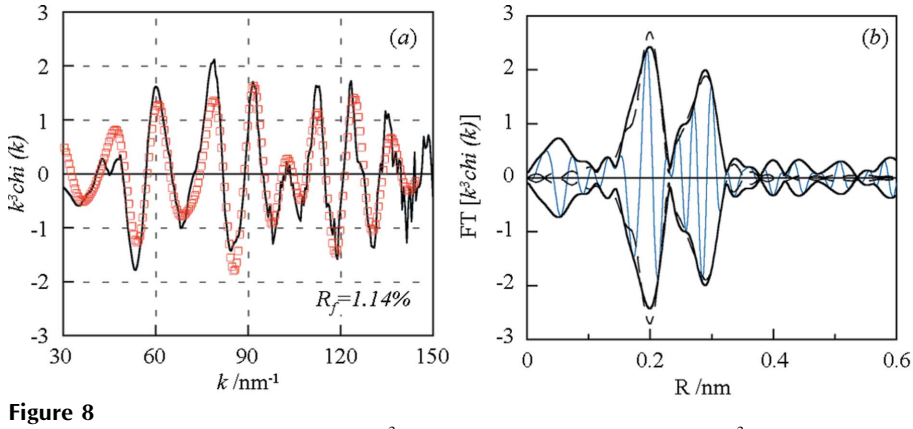

Figure 8
Best-fitting results for the Mo K-edge $\Delta k^3\chi(k)$ (*a*) and Fourier transformed $\Delta k^3\chi(k)$ (*b*) spectra of the NiMo(0.6) catalyst. The spectra were fitted using the Mo–S, Mo–Ni and Mo–Mo coordination shells.

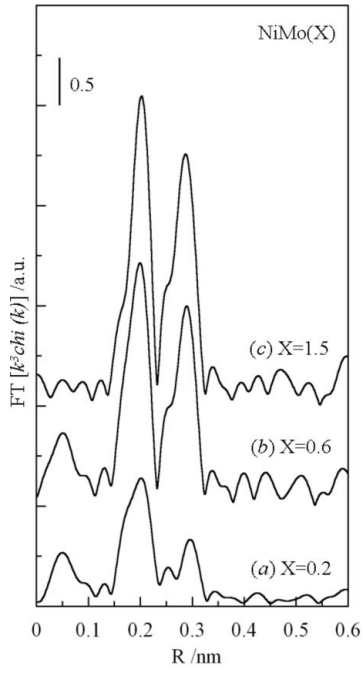

Figure 7
Fourier-transformed Mo K-edge $\Delta k^3\chi(k)$ spectra of the NiMo(X) catalysts. The Mo K-edge $\Delta k^3\chi(k)$ was defined as follows: $\Delta k^3\chi(k)$ = Mo K-edge $k^3\chi(k)$ [NiMo(X)] − Mo K-edge $k^3\chi(k)$ (Mo/Al_2O_3).

3.3. Comparison with carbon-supported catalysts

In the Ni K-edge FT-EXAFS spectra of the NiMo/C catalysts reported previously (Louwers & Prins, 1992), a weak peak assigned to the Ni–Mo coordination shell of the Ni–Mo–S phase was observed at around 0.24 nm (not phase-shift corrected) in their FT-EXAFS spectra. The coordination number and interatomic distance of this coordination shell were reported to lie in the 0.5–1.5 and 0.276–0.277 nm ranges, respectively. The interatomic distance of the Ni–Mo and Mo–Ni coordination shells of the $NiMo/Al_2O_3$ catalyst reported in this paper (Tables 2 and 4) were identical to these reported values within the error of EXAFS measurement, whereas the coordination number was a little bit smaller. However, we cannot definitely conclude that the Ni–Mo coordination number is different between two catalysts because the estimated standard deviation of the coordination number was relatively large.

In the Ni K-edge FT-EXAFS spectra of the NiMo/C catalysts reported previously, an additional peak was observed at around 0.28 nm (not phase-shift corrected). Based on curve-fitting analysis, this peak was assigned to the Ni–Ni coordi-

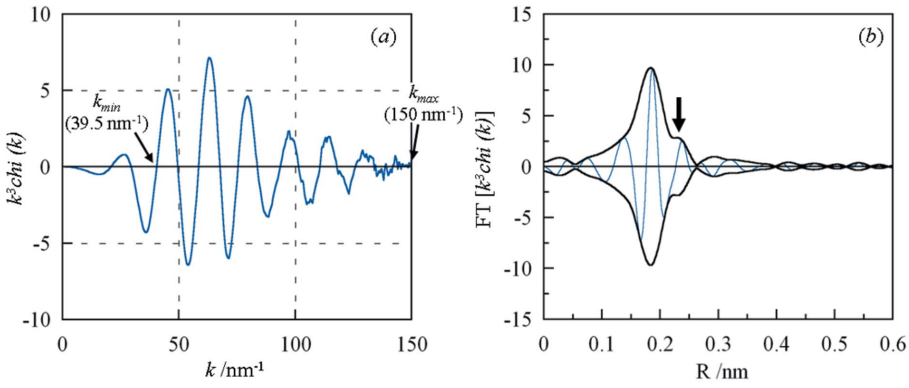

Figure 9
Ni *K*-edge $k^3\chi(k)$ and its FT-EXAFS spectra of the NiMo/C catalyst. The X-ray absorption spectrum was measured at ambient temperature after sulfiding pretreatment at 613 K and 0.1 MPa using the chamber equipped the with PBI windows.

nation shell of the Ni–Mo–S phase. Because the coordination number of this shell was around unity, two Ni atoms are suggested being adjacent on the edge of the MoS_2 species on the carbon-supported catalysts. Interestingly, the corresponding peak was not observed in the Ni *K*-edge FT-EXAFS spectra of the NiMo/Al_2O_3 catalyst shown in this paper. To clarify the reason for this difference, the NiMo/C catalyst was prepared and subjected to Ni *K*-edge EXAFS measurement in this work. EXAFS measurement was conducted at ambient temperature after sulfiding pretreatment at 613 K and 0.1 MPa. The Ni *K*-edge $k^3\chi(k)$ and corresponding FT-EXAFS spectra thus obtained are shown in Fig. 9. These spectra are almost identical to those of the NiMo(0.4) catalyst (*cf.* Fig. 5). No clear peak was observed at around 0.28 nm (not phase-shift corrected) in the FT-EXAFS of the carbon-supported catalyst even after sulfiding pretreatment at atmospheric pressure.

3.4. Structure of the Ni–Mo–S phase

Considering the difference in the FT-EXAFS spectra of the NiMo/C catalyst mentioned above, it is of importance to note that there are two major differences in EXAFS measurement conditions between the current and previous studies. First, the FT range was limited to below 110 nm^{-1} for the Ni *K*-edge $k^3\chi(k)$ of the NiMo/C catalyst reported previously. The limited FT range may be related to the use of the beryllium X-ray windows in the previous study. The other difference is the EXAFS measurement temperature, *i.e.* liquid-N_2 temperature *versus* ambient temperature. To investigate the effect of the FT range, Ni *K*-edge EXAFS measurements were further conducted on the carbon-supported catalyst using the high-pressure chamber equipped with beryllium X-ray windows.

Fig. 10 summarizes the FT-EXAFS spectra of the NiMo/C and NiMo(0.4) catalysts measured using the chamber equipped with PBI and beryllium windows. This figure also includes a representative FT-EXAFS spectrum of the NiMo/C catalyst [(*a*) Ni:Mo molar ratio = 0.3] taken from a previous study (Louwers & Prins, 1992). The NiMo/C catalyst was sulfided at atmospheric pressure in the present study as well, whereas high-pressure sulfiding pretreatment was employed for the NiMo(0.4) catalyst. Note that the spectrum (*b*) was obtained by re-sulfiding of the catalyst used for obtaining the spectrum (*c*). From this figure it is evident that the Ni–Mo coordination peak is weaker when the spectra were measured using the chamber with the beryllium X-ray windows. In other words, a wide FT range leads to a more intense Ni–Mo coordination peak. Furthermore, a new peak was observed at around 0.28 nm (not phase-shift corrected) when the beryllium windows were used. These FT-EXAFS spectra are similar to that reported previously (*a*), even though EXAFS measurements were conducted at a different temperature. On the other hand, only weak peaks were observed at a slightly longer distance (around 0.3 nm, not phase-shift corrected) in the spectra (*c*) and (*e*). These results indicate that the peak at around 0.28 nm in the FT-EXAFS spectra is a ghost peak that is observed only when the FT range is limited to a lower *k* range (<110 nm^{-1}). To make sure of this, curve-fitting analysis was further conducted on the FT-

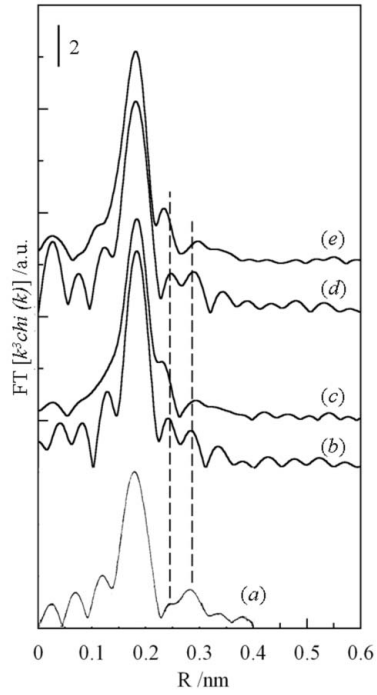

Figure 10
Ni *K*-edge FT-EXAFS spectra of the NiMo/C (*b*, *c*) and NiMo(0.4) (*d*, *e*) catalysts measured using the high-pressure chamber with different types of X-ray windows. X-ray absorption spectra were measured at ambient temperature after sulfiding pretreatment at 613 K and 0.1 MPa (NiMo/C) or 1.1 MPa [NiMo(0.4)]. The FT-EXAFS spectrum of Ni *K*-edge $k^3\chi(k)$ of the NiMo/C taken from Louwers & Prins (1992) is also shown as a reference (*a*). (*b*) Beryllium windows; FT range = 40.0–120 nm^{-1}. (*c*) PBI windows; FT range = 39.5–150 nm^{-1}. (*d*) Beryllium windows; FT range = 40.0–109 nm^{-1}. (*e*) PBI windows; FT range = 39.5–146 nm^{-1}.

Table 5
Fitting results for Ni *K*-edge $k^3\chi(k)$ spectra of the NiMo(0.4) catalyst including a weak peak observed at around 0.3 nm in the FT-EXAFS spectrum.

See Table 1 for explanation of symbols.

Scattering pair	CN	R (nm)	E_0 (eV)†	σ^2 (10^{-5} nm^2)†	N_{idp}	R_f (%)
Ni–O	1.5	0.203	−8.728	1.44	15	1.38
Ni–S	4.9	0.220	−4.213	7.40		
Ni–Ni	0.4	0.246	−2.669	2.81		
Ni–Mo	0.7	0.273	0	3.60		
Ni–Ni	–‡	0.328	−2.669	2.81		

† E_0 and σ^2 were not fitted. ‡ Negative value.

EXAFS spectrum (*e*) [NiMo(0.4) catalyst] including a weak peak at around 0.3 nm (phase shift not corrected) using the Ni–O, Ni–S, Ni–Ni, Ni–Mo and Ni–Ni coordination shells. Optimized structural parameters are summarized in Table 5. Curve-fitting analysis provided a negative value for the second Ni–Ni coordination shell. Furthermore, the R_f value was more than five times greater than that obtained by the fitting analysis without using the second Ni–Ni shell (see Table 2). All these results suggest that an isolated Ni atom is located at the MoS_2 edge site in the Ni–Mo–S phase both on the Al_2O_3- and carbon-supported catalysts.

4. Conclusions

To obtain evidence for the formation of the Ni–Mo–S phase on NiMo/Al_2O_3 catalysts under high-pressure HDS conditions, a high-pressure EXAFS chamber was newly constructed and used to investigate the coordination structure of Ni species on the NiMo/Al_2O_3 catalyst sulfided at high pressure. By using this chamber, Ni *K*-edge $k^3\chi(k)$ spectra of the NiMo/Al_2O_3 catalyst were obtained with higher signal-to-noise ratio over a wide k range, which made it possible to conduct FT of EXAFS spectra over a wide k range (39.5–146 nm^{-1}) compared with Ni *K*-edge EXAFS measurement on the NiMo/C catalysts reported previously.

EXAFS measurement using the newly constructed chamber supported the hypothesis that the Ni–Mo–S phase is formed on the Al_2O_3-supported NiMo catalyst sulfided under high-pressure conditions. The shoulder peak at around 0.24 nm in the Ni *K*-edge FT-EXAFS spectra of the NiMo/Al_2O_3 catalyst is assigned to the Ni–Mo coordination shell of the Ni–Mo–S phase. It was also revealed that the shoulder peak was more intense compared with the FT-EXAFS spectra of the NiMo/C catalyst reported previously, while the interatomic distance and coordination number were comparable. On the other hand, although the Ni–Ni coordination peak of the Ni–Mo–S phase had been observed in previous FT-EXAFS spectra of the NiMo/C catalyst, a corresponding peak was not seen in the FT-EXAFS spectra of the NiMo/Al_2O_3 and NiMo/C catalysts in the present study. Our Ni *K*-edge EXAFS measurement indicated that a ghost peak is observed when FT is conducted over a limited k range ($\sim$110 nm^{-1}), which suggested that an isolated Ni atom is located at the MoS_2 edge site in the Ni–Mo–S phase on NiMo/Al_2O_3 and NiMo/C catalysts.

EXAFS measurements were conducted at the BL9C and NW10A stations at the PF under the approval of PF-PAC (proposal No. 2008G180). EXAFS measurements were also performed at BL14B2 at SPring-8 with the approval of JASRI (proposal No. 2009B1835). We gratefully thank the staff of PF and SPring-8 for their technical support and their kind help.

References

Ankudinov, A. L., Ravel, B., Rehr, J. J. & Conradson, S. D. (1998). *Phys. Rev. B*, **58**, 7565–7576.
Areán, C. O. & Viñuela, J. S. D. (1985). *J. Solid State Chem.* **60**, 1–5.
Boudart, M., Arrieta, J. S. & Betta, R. D. (1983). *J. Am. Chem. Soc.* **105**, 6501–6502.
Bouwens, S. M. A. M., Prins, R., De Beer, V. H. J. & Koningsberger, D. C. (1990). *J. Phys. Chem.* **94**, 3711–3718.
Bouwens, S. M. A. M., van Veen, J. A. R., Koningsberger, D. C., De Beer, V. H. J. & Prins, R. (1991). *J. Phys. Chem.* **95**, 123–134.
Cattaneo, R., Rota, F. & Prins, R. (2001). *J. Catal.* **199**, 318–327.
Chang, C. L., Tao, Y. K., Swinnea, J. S. & Steinfink, H. (1987). *Acta Cryst.* C**43**, 1461–1465.
Clausen, B. S., Topsøe, H., Candia, R., Villadsen, J., Lengeler, B., Als-Nielsen, J. & Christensen, F. (1981). *J. Phys. Chem.* **85**, 3868–3872.
Clausen, B. S., Topsøe, H. & Massoth, F. E. (1996). *Catalysis Science and Technology*, Vol. 11, edited by J. R. Anderson and M. Boudart. New York: Springer.
Dalla Betta, R. A., Boudart, M. & Foger, K. (1984). *Rev. Sci. Instrum.* **55**, 1910–1913.
Dickinson, R. G. & Pauling, L. (1923). *J. Am. Chem. Soc.* **45**, 1466–1471.
Dugulan, A. I., Crajé, M. W. J. & Kearley, G. J. (2004). *J. Catal.* **222**, 281–284.
Dugulan, A. I., Hensen, E. J. M. & van Veen, J. A. R. (2008). *Catal. Today*, **130**, 126–134.
Fujikawa, T., Kimura, H., Kiriyama, K. & Hagiwara, K. (2006). *Catal. Today*, **111**, 188–193.
Grunwaldt, J.-D., Ramin, M., Rohr, M., Michailovski, A., Patzke, G. R. & Baiker, A. (2005). *Rev. Sci. Instrum.* **76**, 1–7.
Jentoft, R. E., Deutsch, S. E. & Gates, B. C. (1996). *Rev. Sci. Instrum.* **67**, 2111–2112.
Kampers, F. W. H., Maas, T. M. J., Van Grondelle, J., Brinkgreve, P. & Koningsberger, D. C. (1989). *Rev. Sci. Instrum.* **60**, 2635–2638.
Kasahara, S., Koizumi, N., Iwahashi, J. & Yamada, M. (1994). *Sekiyu Gakkaishi*, **38**, 345–352.
Koizumi, N., Iijima, M., Kasahara, S. & Yamada, M. (1996). *Chem. Lett.* **9**, 815–816.
Koizumi, N., Yamazaki, M., Hatanaka, S. & Yamada, M. (1997). *Catal. Today*, **39**, 33–44.
Koizumi, N., Yamazaki, M., Iijima, M. & Yamada, M. (1997). *Appl. Surf. Sci.* **121–122**, 429–432.
Louwers, S. P. A. & Prins, R. (1992). *J. Catal.* **133**, 94–111.
Nicosia, D. & Prins, R. (2005). *J. Catal.* **231**, 259–268.
Nowack, E., Schwarzenbach, D. & Hahn, Th. (1991). *Acta Cryst.* B**47**, 650–659.
Okamoto, Y., Ishihara, S.-Y., Kawano, M., Satoh, M. & Kubota, T. (2003). *J. Catal.* **217**, 12–22.
Parise, J. B. (1980). *Acta Cryst.* B**36**, 1179–1180.
Rooksby, H. P. (1948). *Acta Cryst.* **1**, 226.
Roy, M. & Gurman, S. J. (1999). *J. Synchrotron Rad.* **6**, 228–230.
Shirai, M., Nomura, M., Asakura, K. & Iwasawa, Y. (1995). *Rev. Sci. Instrum.* **66**, 5493–5498.

Stern, E. A. (1993). *Phys. Rev. B*, **48**, 9825–9827.
Swanson, H. E. & Tatge, E. (1953). *Natl. Circ.* **1**, 13.
Topsøe, H. & Clausen, B. S. (1984). *Catal. Rev. Sci. Eng.* **26**, 395–420.
Topsøe, H., Clausen, B. S., Candia, R., Wivel, C. & Mørup, S. (1981). *J. Catal.* **68**, 433–452.
Topsøe, H., Clausen, B. S., Topsøe, N.-Y. & Pedersen, E. (1986). *Ind. Eng. Chem. Fundam.* **25**, 25–36.
Wivel, C., Candia, R., Clausen, B. S., Mørup, S. & Topsøe, H. (1981). *J. Catal.* **68**, 453–463.
Yamada, M., Koizumi, N. & Yamazaki, M. (1999). *Catal. Today*, **50**, 3–8.